



Exploring the Hydrogen Abstraction Pathway in HOM Formation from α -pinene Photooxidation Systems under Varying NO Conditions

5 Hui Wang^{1†}, Hongru Shen^{2†}, Defeng Zhao^{3,4*}, Sungah Kang¹, Rongrong Wu⁵, Yarê Baker⁶, Quanfu He⁷, Annika Zanders¹, Mathias Bachner⁸, Douglas R. Worsnop^{9,10}, Thorsten Hohaus¹, Thomas F. Mentel¹¹, Sören R. Zorn^{1*}

¹ Institute of Climate and Energy Research, ICE-3: Troposphere, Forschungszentrum Jülich, 52425 Jülich, Germany.

² School of Environmental Science and Engineering, Shanghai Jiao Tong University, Shanghai 200240, P. R. China

10 ³ Shanghai Frontiers Science Center of Atmosphere-Ocean Interaction, Department of Atmospheric and Oceanic Sciences & Institute of Atmospheric Sciences, Fudan University, Shanghai 200438, China.

⁴ Institute of Eco-Chongming (IEC), 20 Cuiniao Rd., Chongming, Shanghai, 202162, China.

⁵ Centre for Atmospheric Sciences, School of Earth, Atmospheric & Environmental Sciences, University of Manchester, M13 9PL Manchester, United Kingdom.

15 ⁶ Leibniz Institute for Tropospheric Research (TROPOS), 04318 Leipzig, Germany

⁷ Earth, Ocean and Atmospheric Sciences (EOAS) Thrust, Function Hub, The Hong Kong University of Science and Technology (Guangzhou), 511458 Guangzhou, Guangdong, China

⁸ Institute of Technology and Engineering, Forschungszentrum Jülich, 52425 Jülich, Germany.

20 ⁹ Institute for Atmospheric and Earth System Research/Physics, Faculty of Science, University of Helsinki, 00560 Helsinki, Finland.

¹⁰ Aerodyne Research, Inc., Billerica, 01821 Massachusetts, United States.

¹¹ Present Address: Keplerstrasse 13, 35390 Gießen, Germany

† These authors contributed equally to this work.

Correspondence to: Sören R. Zorn (s.zorn@fz-juelich.de) and Defeng Zhao (dfzhao@fudan.edu.cn)



Abstract. Highly oxygenated organic molecules (HOM) are formed via autoxidation during ·OH initiated oxidation of α-pinene. We investigated the importance of ·OH addition and hydrogen (H)-abstraction in HOM formation from α-pinene photooxidation under varying NO concentrations. HOM-RO₂· and subsequent termination products were detected by chemical ionization mass spectrometry. In the absence of NO, C₁₀H₁₇O_x· peroxy radicals and related products dominated the HOM spectrum, contributing >70%. In contrast, the presence of NO induced substantial changes in HOM products, particularly the rapid formation of C₁₀H₁₅O_x·-related HOM, such as C₁₀H₁₅NO₈. This indicates an enhanced contribution from the H-abstraction pathway. The ratio of C₁₀H₁₅NO_x to C₁₀H₁₇NO_x also increased significantly from 0.34 to 0.84 as the initial loss rate of RO₂· via reaction with NO rose from 0.18 s⁻¹ to 1.7 s⁻¹. Under high NO conditions (7.4 ppbv), major C₁₀H₁₅O_x·-related closed-shell HOM (C₁₀H₁₄O_x and C₁₀H₁₅NO_x) contributed ~30% to the total HOM. Fuzzy c-means clustering identified C₁₀H₁₅O_x·-related HOM, thought to be second generation products via pinonaldehyde formation, as the cluster with the fastest formation rate, consistent with first-generation products. Subsequent pinonaldehyde oxidation experiments under comparable conditions showed significantly different product distributions. Formation of C₁₀H₁₅O_x·-related HOM in α-pinene experiments was more than two times higher than in the pinonaldehyde experiments despite the pinonaldehyde turnover being more than ten times lower. This study highlights the significance of the H-abstraction pathway for ·OH initiated α-pinene photooxidation in the presence of NO, exploring detailed product distributions formed via this pathway.

45 Key Words: highly oxygenated organic molecules (HOM), hydrogen-abstraction, simulation chamber, clustering, chemical ionization mass spectrometer (CIMS)



1. Introduction

Secondary organic aerosols (SOA) in the atmosphere contribute significantly to particulate matter in the PM₁ size range and can affect regional air quality, human health and global radiative forcing (Jimenez et al., 2009; Peng et al., 2016). The oxidation of biogenic volatile compounds (BVOC) contributes significantly to the total formed SOA. Highly oxygenated organic compounds (HOM) are produced via autoxidation of peroxy radicals (RO₂·). They typically contain at least six oxygen atoms and consequently show a low to extremely low volatility. This enables them to nucleate or to condense onto existing particles and thus to significantly contribute to SOA formation (Bianchi et al., 2019; Mentel et al., 2015; Ehn et al., 2014).

α -pinene is globally the most abundant monoterpene and has been shown to form significant amounts of HOM when oxidized by O₃ or by hydroxyl radicals (·OH) (Ehn et al., 2014; Berndt et al., 2016). ·OH initiated oxidation of α -pinene occurs primarily via the OH-addition pathway (~90%) or the hydrogen (H)-abstraction pathway (~10%). Major products of the latter are RO₂· radicals with the formulas C₁₀H₁₇O₃· and C₁₀H₁₅O₂· (Vereecken et al., 2007).

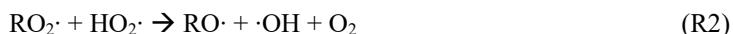
The OH-addition pathway is known to effectively form HOM with fast rates when the six-membered ring is broken (Berndt, 2021; Xu et al., 2019). However, the potential role of the H-abstraction pathway for HOM formation has received far less attention and was thought to be negligible until Shen and coworkers suggested its significant contribution to HOM (Shen et al., 2022). In addition, Luo et al. (2023) also highlighted the significance of H-abstraction to HOM formation from limonene photooxidation in the presence of NO. Therefore, the H-abstraction pathway can be a potential explanation for the observations in Hyytiälä where C₁₀H₁₅O_x-related HOM species (e.g. C₁₀H₁₅NO₈) are dominant and have been identified as fingerprints of daytime oxidation (Yan et al., 2016). However, confirmation and clarification of the contribution of the H-abstraction pathway to HOM formation are still required. In the study by Shen et al. (2022) the potential role of the conversion of pinonaldehyde to C₁₀H₁₅O_x· species was only estimated and not directly measured. The extent to which pinonaldehyde oxidation contributes to C₁₀H₁₅O_x-related HOM in α -pinene systems remains uncertain.

According to Vereecken et al. (2007), the detection of C₁₀H₁₅O_x related products with fewer than five oxygen atoms would be a strong indicator for H-abstraction. However, Shen et al. (2022) reported only products and in particular HOM with oxygen numbers greater than six. Also, NO was present in all experiments performed by Shen and coworkers (Shen et al., 2022). The presence or absence of NO can have a significant impact, as it strongly influences the rearrangement of alkoxy radicals, which is crucial to facilitate HOM formation via the H-abstraction pathway (Shen et al., 2022). Therefore, systematic experiments under varying NO conditions are essential for confirming the occurrence of the H-abstraction pathway, to elucidate its product distribution, and to clarify its role in HOM and subsequent SOA formation in α -pinene photooxidation systems.

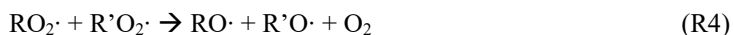
Competition between termination pathways of C₁₀H₁₇O_x· and C₁₀H₁₅O_x· peroxy radicals determines the product distributions in α -pinene photooxidation systems (Mentel et al., 2015). All products are separated into various families based on the numbers of carbon atoms, hydrogen atoms and oxygen atoms. The C₁₀H₁₈O_x family, which includes compounds containing ten carbon atoms, eighteen hydrogen atoms, and a varying number of oxygen atoms with hydroperoxide or



alcohol functions, can only be attributed to $C_{10}H_{17}O_x\cdot$ via termination either by $HO_2\cdot$ radicals (Reaction R1) or by other $RO_2\cdot$ (Reaction R3; (Baker et al., 2024)). Similarly, the organic nitrate $C_{10}H_{17}NO_x$ family is formed via the reaction of $C_{10}H_{17}O_x\cdot$ with NO (Reaction R6) (Berndt, 2021). The $C_{10}H_{14}O_x$ family, comprising carbonyl containing compounds, is generated
85 either via reactions of $C_{10}H_{15}O_x\cdot$ with other peroxy radicals or via self-termination (Reaction R8; (Rissanen et al., 2014)). In the atmosphere, alkoxy radicals with the formula $C_{10}H_{15}O_{x-1}\cdot$ are mainly products of the reaction between $C_{10}H_{15}O_x\cdot$ and NO (Reaction R2; (Berndt, 2021)). The $C_{10}H_{15}NO_x$ family is uniquely attributed to the reaction of $C_{10}H_{15}O_x\cdot$ peroxy radicals with NO (Reaction R6). Thus, the appearance of HOM with formulas $C_{10}H_{18}O_x$ and $C_{10}H_{17}NO_x$ can clearly be traced to $C_{10}H_{17}O_x\cdot$, while $C_{10}H_{14}O_x$ and $C_{10}H_{15}NO_x$ are clearly related to $C_{10}H_{15}O_x\cdot$. The formation of the $C_{10}H_{16}O_x$ family can occur
90 via multiple pathways including termination reactions of $C_{10}H_{15}O_x\cdot$ with $HO_2\cdot$ or other $RO_2\cdot$ radicals, termination of $C_{10}H_{17}O_x\cdot$ with other $RO_2\cdot$, or self-termination of $C_{10}H_{17}O_x\cdot$. The important termination pathways of $RO_2\cdot$ and corresponding products are shown below and in **Figure 1**.

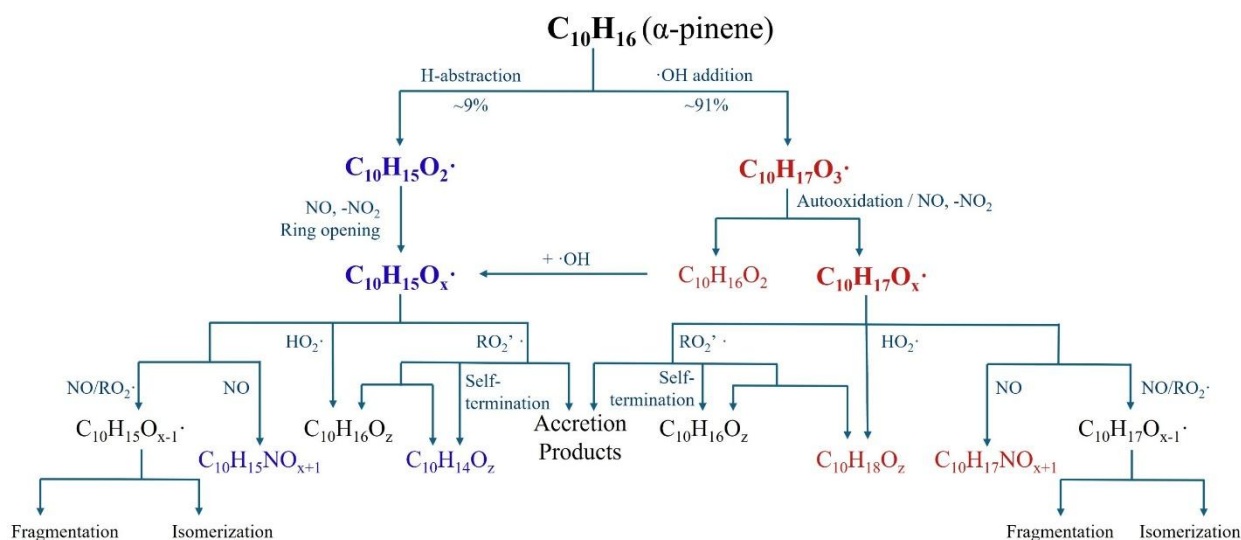


95



100





105 **Figure 1.** A schematic diagram illustrating $\cdot\text{OH}$ initiated α -pinene photooxidation through either the OH-addition pathway or the H-abstraction pathway. The unique peroxy radicals and their subsequent termination reactions are also depicted. The potential closure products are categorized into different families based on their formation pathways and the number of hydrogen atoms in molecules.

In our study we conducted systematic experiments of α -pinene photooxidation under varying NO concentrations to investigate the role of the H-abstraction pathway in HOM formation. We focused on early reaction stages which means the first minutes after $\cdot\text{OH}$ generation by photolysis of H_2O_2 , to capture primary generation product distributions, when only autoxidation and reaction with NO were the two dominant reaction pathways for $\text{RO}_2\cdot$. Fuzzy c-means clustering was applied to distinguish $\text{C}_{10}\text{H}_{15}\text{O}_x\cdot$ -related HOM from other products based on their formation pathways. To separate the role of secondary oxidation, pinonaldehyde was investigated under identical conditions, and the results were compared with the α -pinene system. Both less oxygenated and highly oxygenated products were detected using propylamine and nitrate as reagents ions by two chemical ionization mass spectrometers (CIMS).

Combination of the results provides complementary and consistent insights into product distributions and formation pathways. The results demonstrate that the H-abstraction pathway is an important process generating product distributions highlighting its potential contribution to HOM and SOA formation.

2. Experiments and Methods

120 2.1 Simulation experiments in SAPHIR STAR

The experiments were conducted in SAPHIR-STAR, a 2 m^3 continuously stirred tank reactor (SAPHIR: Simulation of Atmospheric PHotochemistry In a large Reaction chamber; STAR: - STirred Atmospheric flow Reactor).¹⁵ The details about its basic concept of operation have been described previously (Mentel et al., 2009; Baker et al., 2024). For this study the system was operated with a total flow rate of 60 L min^{-1} , of which 32 L min^{-1} were injected into the reactor, resulting in a



125 residence time of approximately 60 minutes. Experimental conditions were maintained at 20 °C and at 20% relative humidity. ·OH radicals were produced by photolyzing hydrogen peroxide (H₂O₂) using two 254 nm UV-C lamps (TUV 16W 4P SE, Philips). The photolysis rate was controlled by reducing the photon flux by covering part of the lamps with adjustable bellows. H₂O₂ vapor was introduced into SAPHIR-STAR by bubbling a 0.2 L min⁻¹ nitrogen (N₂) flow through a 30% w/w H₂O₂ solution (Sigma-Aldrich).

130 In the α-pinene photooxidation experiments a continuous flow of 0.012 L min⁻¹ from an α-pinene cylinder (with a concentration of ~ 48.8 ppm) was injected into SAPHIR-STAR resulting in an initial concentration of ~10 ppbv. For pinonaldehyde photooxidation, liquid pinonaldehyde (Orgentis chemicals, 99.7%) was introduced by use of a syringe pump (Fusion 4000, Chemyx Inc.) at a flow rate of 0.145 μL h⁻¹ resulting in a concentration of 5 ppbv of pinonaldehyde in the reactor. NO was injected into the chamber from a gas cylinder (20.09 ppm NO in N₂ 5.0) via a mass flow controller for
135 initial concentrations before reaction ranging between 0 and 7.5 ppbv.

To investigate the role of the H-abstraction pathway in α-pinene photooxidation we focused on the early stages of the reaction systems before secondary-generation products become important. All precursors were injected into the dark chamber. Once all precursors were well mixed and showed stable concentrations the UV-C lamps were switched on for ·OH production by photolysis. The UV-C lamps were then kept on at a constant setting for one hour to initialize the
140 photooxidation of α-pinene, followed by three hours without irradiation to allow for products to be flushed out and for precursors to recover initial concentrations. This cycle was repeated three times for every system investigated.

During the early stages of the photooxidation cycle the dominant reactions of RO₂· radicals are either isomerization or reactions with NO. Since the amount of NO available for reaction is crucial we defined the end of the early reaction stage as the time when the NO concentration decreased below ~ 1 ppbv. Based on the NO and HO₂· concentrations shown in **Table 1**,
145 and with $k_{[\text{RO}_2][\text{HO}_2]} = 1.85 \cdot 10^{-11} \text{ cm}^3 \text{ s}^{-1}$ and $k_{[\text{RO}_2][\text{NO}]} = 1 \cdot 10^{-11} \text{ cm}^3 \text{ s}^{-1}$ applied (Baker et al., 2024; Berndt et al., 2016; Jenkin et al., 1997), the ratio of $k_{[\text{RO}_2][\text{NO}]}[\text{NO}]$ to $k_{[\text{RO}_2][\text{HO}_2]}[\text{HO}_2\cdot]$ is ~ 10 for early reaction stages under low NO and high NO conditions. Therefore, the first 100 seconds were defined as early reaction stage for the low-NO case (0.91±0.05 ppbv), and the first 300 seconds for the high-NO case (7.4±0.05 ppbv), respectively. For the no-NO case a time window of 100 seconds was used comparable the one of the low-NO case.

150 Since the first hour of photooxidation is crucial for investigating the relative role of the H-abstraction channel compared to the OH-addition channel, a cycle of one hour of photolysis followed by three hours without irradiation was repeated three times for each experimental condition listed in **Table 1**, as mentioned before. The time series of α-pinene, H₂O₂, and C₁₀H₁₇O₇· peroxy radicals over a total run of the experiments (14 hours) are shown in **Figure S1**, together with an example of the experimental procedure. During the final cycle the lamps were kept on continuously for 6 hours to allow the system to
155 reach steady state.



2.2 Methods and instrumentation

Instrumentation

The α -pinene concentration was measured by a proton-transfer-reaction mass spectrometry (PTR-TOF-MS, Ionicon Analytik GmbH). Gas concentrations of NO and NO_x were detected by a NO monitor (NCLD899, Eco Physics GmbH) coupled to a self-built photolytical NO₂ converter. H₂O was monitored by a Picarro CRDS analyzer (G2401, Picarro Inc.).

An Eisele type inlet (Eisele and Tanner, 1993) was coupled to an atmospheric-pressure-interference time-of-flight mass spectrometer (Api-TOF-MS, Tofwerk AG) using a positive reagent ion (C₃H₇NH₃⁺) produced from propylamine (C₃H₇NH₂, ≥ 99 %, Sigma Aldrich) to ionize less oxygenated organic products in gas phase (Berndt et al., 2018). The resolution of this instrument was ~ 3500 m/Δm FWHM for m/z larger than 150. C₃H₇NH₃⁺ has the advantage that it does cluster with pinonaldehyde very efficiently, which is vital for investigating α -pinene related systems since pinonaldehyde is a major oxidation product and a representative for the OH-addition pathway. The sensitivity of pinonaldehyde (**Figure S2**) was calibrated in propylamine CIMS (amine-CIMS) by using a Liquid Calibration Unit (LCU, Ionicon Analytik GmbH). The long TOF-MS (LTOF, Tofwerk AG), with a resolution ~8500 m/Δm FWHM for masses larger than 200 Th, was coupled with a multi-scheme ionization inlet (MION, Karsa Oy) (Rissanen et al., 2019). The MION inlet allows switching between bromide and nitrate modes, utilizing Br⁻ and NO₃⁻ as reagent ions, respectively. The Br⁻ was mainly used to detect HO₂· radicals and their relative change (Albrecht et al., 2019). NO₃⁻ CIMS has been shown to efficiently detect HOM (Ehn et al., 2014). Wang et al. have also shown that HOM(NO₃⁻) clusters with four or more oxygen atoms in the HOM have a higher bonding strength than the H₂SO₄(NO₃⁻) cluster (Wang et al., 2024), possibly due to the multiple hydroperoxyl and hydroxy functional groups present in HOM molecules (Bianchi et al., 2019). This indicates a relative sensitivity at the collision limit for these highly functionalized HOM. Since the study by Wang and coworkers (Wang et al., 2024) used the same setup regarding instrument and inlet we assumed that the MION-CIMS used in this study detects HOM compound with same sensitivity. All CIMS data were processed using the IGOR Pro (WaveMetrics) based Tofware v3.3.0.

·OH concentration, VOC turnover and HO₂· concentration

The concentration of ·OH radicals was calculated based on the reacted fraction of α -pinene respectively pinonaldehyde under steady-state conditions (**Eq.1**) (Kiendler-Scharr et al., 2009), meaning that all parameter are stable and the injection rate equals the loss rate. In **Eq.1**, F represents the total flow through the chamber, and V is the volume of chamber. [VOC]₀ and [VOC]_{SS} represent the VOC concentration in the dark and in steady state (SS), respectively. k_{OH} denotes the rate constants for the reaction of α -pinene or pinonaldehyde with ·OH radicals, which are 5.4·10⁻¹¹ cm³ s⁻¹ and 4.0·10⁻¹¹ cm³ s⁻¹ at 20 °C, respectively (Atkinson and Arey, 2003; Rolletter et al., 2020). The estimated ·OH concentrations are listed in **Table 1**. The turnover of VOC by ·OH can be calculated using **Eq.2**, which represents the amount of VOC consumed by the reaction with ·OH (Baker et al., 2024).

$$[\cdot OH]_{SS} = \frac{\frac{F}{V} \times \frac{[VOC]_0 - [VOC]_{SS}}{[VOC]_{SS}}}{k_{OH}} \quad \text{Eq.1}$$



190

$$\text{turnover}_{\text{voc}} = k_{\text{OH}} \times [\text{VOC}]_{\text{SS}} \times [\cdot\text{OH}]_{\text{SS}} \quad \text{Eq.2}$$

To determine the concentrations of HO₂· in the chamber, a series of isoprene photooxidation experiments was conducted, and a corresponding box model based on the MCM v3.3.1 chemistry, which used the same boundary conditions, was applied. More details about the box model can be found in Baker et al (Baker et al., 2024).

195 In these experiments, a continuous flow of 0.050 L/min of isoprene from a gas cylinder (11.8 ± 0.24 ppmv, Linde GmbH) was introduced into the chamber to achieve a target concentration of 10 ppbv before reactions. The UV-C lamps were then adjusted in five different steps by varying the lamp bellows to vary [·OH]_{SS}. The box model reproduced both [isoprene]_{SS} and [·OH]_{SS} for each step within the measurement uncertainties (**Figure S3**). A linear fit was applied to normalized HO₂·/[Br + (H₂O)Br] (in ncps) and modelled [HO₂·]_{SS} (**Figure S4**), and the slope was used as calibration factor for calculating HO₂·
200 levels in subsequent experiments (**Table 1**).

Fuzzy c-means clustering (FCM)

Hierarchical clustering has been shown to be an effective dimensionality-reduction technique to identify major ion groups and patterns of chemical behavior in mass spectrometry previously (Koss et al., 2020). Wu et al. demonstrated the application of the soft clustering method FCM for simplifying complex mass spectrometric data to reveal chemical and
205 kinetic characteristics of chemical reaction systems (Wu et al., 2024). Here, FCM was applied to mass spectrometric data to explore the formation rates of a variety of products along competing reaction channels. The time series of 156 ions in the early reaction stage (up to 3000 s after start of the photooxidation processes) were selected for clustering. Herein, the major ions from both nitrate-CIMS and amine-CIMS were combined. Normalization was applied to all ions used since their typical time behavior was more important for clustering than their absolute abundance. Initially, all ion signals were normalized
210 relative to their corresponding reagent ions. Subsequently, Frobenius normalization was applied to each ion across the entire time range.

Three parameters were calculated to help to constrain the optimal number of clusters: sum of squared errors (SSE), distortions, and silhouette coefficient (Wu et al., 2024; Campello and Hruschka, 2006). The FCM algorithm was run 50 times for each cluster number in a range between 2 to 13. The results of the three parameters as function of cluster numbers
215 are shown in **Figure S5**. The four-cluster solution was then selected for the subsequent analysis.



3. Results and Discussion

3.1 C₁₀H₁₅O_x-related HOM form rapidly from α-pinene photooxidation in the presence of NO

All major products from α-pinene photooxidation that were detected by NO₃⁻ CIMS, in the absence or presence of NO, were categorized into the following groups: C₁₀ monomers, C₂₀ dimers, and C_{<10} fragments. The time series for contributions of each group varies for the three different NO conditions, as shown in **Figure 2 (a-1, a-2, a-3)**. A comparison under varying NO conditions is critical to elucidate the role of NO, since the presence of NO, ring opening and isomerization of alkoxy radicals, can be crucial in facilitating HOM formation from H-abstraction channel (Shen et al., 2022). The analysis was focused on the early reaction stages to explore the importance of the H-abstraction channel for HOM formation. The average product distributions of C₁₀ monomers from early stage α-pinene photooxidation without and with NO are illustrated by Kendrick Mass Defect (KMD) plots as a function of oxygen number (Kendrick Mass = oxygen, **Figure 2 (b-1, b-2, b-3)**). Each plot features seven distinct families, with compounds in each family sharing the same carbon and hydrogen numbers but differing in oxygen content.

Table 1. Overview of experimental conditions: pinonaldehyde photooxidation without NO (P0) and with high NO (PN_{high}), α-pinene photooxidation without NO (A0), with low NO (AN_{low}), and with high NO (AN_{high}). The precursor concentrations in the dark and in photooxidation steady-state conditions are shown at t₀ and t_s, respectively. The measurement uncertainty is less than 5%. Details about how to estimate ·OH and HO₂· radicals are mentioned in Section 2.2.

no-		VOC		NO (ppbv)	·OH (# cm ⁻³)	HO ₂ · (# cm ⁻³)	Under NO
		pinonaldehyde (ppbv)	α-pinene (ppbv)				
P0	t ₀	1.5	-	0	-	-	
	t _s	0.75	-	0	6.5×10 ⁶	6.4×10 ⁸	
PN _{high}	t ₀	1.8	-	7.0±0.13	-	-	
	t _s	0.75	-	0.36±0.01	9.3×10 ⁶	2.7×10 ⁸	
A0	t ₀	-	10.3±1.7	0	-	-	
	t _s	0.01	8.3±1.4	0	1.25×10 ⁶	3.1×10 ⁸	
AN _{low}	t ₀	-	11.1±1.3	0.91±0.05	-	-	
	t _s	0.05	5.5±1.7	0.05±0.01	5.1×10 ⁶	9.8×10 ⁸	
AN _{high}	t ₀	-	10.6±1.3	7.4±0.05	-	-	
	t _s	0.09	4.2±2.1	0.16±0.01	7.5×10 ⁶	1.0×10 ⁹	

conditions (A0) the relative contributions of C₁₀H₁₈O_x, C₁₀H₁₆O_x, and C₂₀H₃₄O_x are 56.1%, 11.1%, and 8.8%, respectively, and they are all closed-shell products related to C₁₀H₁₇O_x·. The first generation peroxy radicals with four-member ring-opening, C₁₀H₁₇O₃·, can undergo fast unimolecular reactions with rates of 4 ± 2 s⁻¹ (Xu et al., 2019). As shown in **Figure 2(b-1)**, species with the formula C₁₀H₁₇O₇· are identified as predominantly HOM peroxy radicals and are detected in the nitrate mass spectra as C₁₀H₁₇O₇(NO₃)·. This agrees with previous observations by Berndt et al, which were obtained using



four different reagent ions (Berndt, 2021), and calculations by Piletic and Kleindienst (Piletic and Kleindienst, 2022).
240 Additional HO₂[·] radicals are produced in our experiments via the reaction of the ·OH radical with H₂O₂. The increasing
contribution of C₁₀H₁₈O_x (**Figure 2(1-a)**) indicates a significant termination reaction of RO₂[·] by HO₂[·]. Among the C₁₀H₁₈O_x
family, C₁₀H₁₈O₇ shows the highest intensity and is likely produced via termination reactions of C₁₀H₁₇O₇[·] with HO₂[·], which
aligns with the dominance of C₁₀H₁₇O₇[·] in the C₁₀H₁₇O_x[·] family. Compounds with six oxygen atoms but one hydrogen less or
one more hydrogen than C₁₀H₁₇O₇[·] (i.e., C₁₀H₁₆O₆ and C₁₀H₁₈O₆) are significant contributors to total product signals.
245 Compounds with the formula C₁₀H₁₆O₆ likely have carbonyl functionalities and are formed either directly from reaction 3 or
from self-termination reactions of C₁₀H₁₇O₇[·] (Reaction R8) (Iyer et al., 2018; Jenkin et al., 2019).

The appearance of compounds with C_{<10} indicates the formation of alkoxy radicals, since alkoxy radicals can fragment to
form species with less than ten carbon atoms. C₁₀H₁₈O₆ species are possibly alcohols formed from C₁₀H₁₇O₇[·] via reaction 3,
or more likely hydroperoxides derived from C₁₀H₁₇O₆[·] via reaction 1 (Iyer et al., 2018; Jenkin et al., 2019). In addition to C₁₀
250 HOM monomers, C₂₀ accretion products also significantly contribute to HOM, particularly species containing 8, 10, or 12
oxygen atoms (**Figure S6**). These have been identified as the most abundant dimers from ·OH initiated α-pinene
photooxidation system by Berndt et al (Berndt et al., 2016). C₂₀H₃₄O_(8,10,12) can be mechanistically explained by
recombination of C₁₀H₁₇O₇[·] with C₁₀H₁₇O₃[·], C₁₀H₁₇O₅[·], or another C₁₀H₁₇O₇[·] via reaction 4. C₁₀H₁₇O_(3,5,7)[·] have previously
been reported to dominate the product spectrum (Lee et al., 2023; Berndt, 2021). In summary, the obtained HOM
255 distributions in the base case without NO addition (A0) are consistent with previous studies and show mechanistically
reasonable results.

When reactions are initiated in the presence of NO (see experiments AN_{low} and AN_{high} in **Table I**), the product distribution
in the early reaction stage (when the RO₂[·] + NO regime is dominant) differs significantly from the no-NO cases (A0). The
C₁₀H₁₇NO_x product family, identified as organic nitrates, accounts for 29.9% and 29.4% of the total signal under low NO and
260 high NO conditions, respectively, and dominates C₁₀H₁₇O_x[·]-related HOM families. The most abundant species with formulas
C₁₀H₁₇NO_(6,7,8) most likely represent organic nitrates formed via reactions of C₁₀H₁₇O_(5,6,7)[·] with NO. As the initial NO
concentration increases, contribution from C₁₀H₁₇O₆[·]-derived HOM, such as C₁₀H₁₇NO₇ and C₁₀H₁₈O₆, also rises (**Figure
S7**). When the initial NO increased from 0.91±0.05 to 7.4±0.05 ppbv, the ratios of C₁₀H₁₇NO₇ to C₁₀H₁₇NO₈ and C₁₀H₁₈O₆ to
C₁₀H₁₈O₇ are enhanced from 0.32 to 0.43 and from 0.63 to 0.78, respectively. At least one alkoxy step (reaction 7) is
265 necessary to produce peroxy radicals with even number, e.g. C₁₀H₁₇O₆[·]. Therefore, the presence NO promotes the occurrence
of alkoxy steps in HOM formation. Compared to the A0 condition, the contributions of accretion products with C₂₀H₃₄O_(9,11)
are also promoted. For forming C₂₀H₃₄O_(9,11) via reaction 5 an C₁₀H₁₇O_x[·] peroxy radical with an even oxygen number must be
involved, e.g. C₁₀H₁₇O₄[·] and C₁₀H₁₇O₆[·], further highlighting the role of alkoxy steps in HOM formation.

In addition to the change of C₁₀H₁₇O_x[·]-related HOM, C₁₀H₁₅O_x[·]-related HOM families emerge once NO is introduced into
270 the system (**Figure 2(a-2, a-3, b-2, b-3)**). In the no-NO_x case neither the C₁₀H₁₅NO_x nor the C₁₀H₁₄O_x family contributes
more than 2%. However, under low NO conditions their contribution rises to 10.3% and 4.7%, respectively, and further
increases to 24.9% and 6.0% under high NO conditions. The most abundant peroxy radical in C₁₀H₁₅O_x[·] family is C₁₀H₁₅O₇[·],



as shown in **Figure S7**, followed by $C_{10}H_{15}O_9$, which is consistent with the closed shell organic nitrate distribution, where $C_{10}H_{15}NO_8$ is most prevalent, followed by $C_{10}H_{15}NO_{10}$. The $C_{10}H_{14}O_x$ family contains products with carbonyl groups and is
275 formed via self-termination reactions of peroxy radicals. In addition to C_{10} monomers, accretion products with the formula $C_{20}H_{30}O_x$ and $C_{20}H_{32}O_x$, derived from reaction R5, also increase with elevated NO concentrations. Here at least one peroxy radical containing 15 hydrogen atoms must be involved (Berndt et al., 2018). Compared to monomers, formation of accretion products is reduced since in early stages of the reactions the $RO_2 \cdot + R'O_2 \cdot$ pathway is less important compared to the $NO + RO_2 \cdot$ pathway or the $RO_2 \cdot$ autoxidation. The intensity of $C_{10}H_{16}O_7$ increases gradually until it surpasses that of
280 $C_{10}H_{16}O_6$, which in the absence of NO is the most abundant peak. $C_{10}H_{16}O_7$ is likely a carbonyl compound (or family), formed either through reaction R3, or from self-termination. Both need $C_{10}H_{17}O_8 \cdot$ as precursors. However, analysis of the closed-shell families $C_{10}H_{18}O_x$ and $C_{10}H_{17}NO_x$ indicates the absence of significant formation of $C_{10}H_{17}O_8 \cdot$ in presence of NO, which also aligns with Berndt (Berndt, 2021) and Piletic and Kleindienst (Piletic and Kleindienst, 2022). $C_{10}H_{16}O_7$ may also be a hydroperoxide produced via reaction R2, or an alcohol produced via reaction R3, with $C_{10}H_{15}O_7 \cdot$ peroxy radicals or
285 $C_{10}H_{15}O_8 \cdot$ peroxy radicals serving as precursors. Products formed via $RO_2 \cdot + RO_2 \cdot$ reactions were produced at significantly slower rates than other species, as will be discussed in Section 3.2. Additionally, when $C_{10}H_{15}O_7 \cdot$ reacts with another $RO_2 \cdot$ radical, it forms $C_{10}H_{16}O_6$ or $C_{10}H_{14}O_6$ rather than $C_{10}H_{16}O_7$. Thus, reaction R3 was considered to not contribute significantly, and the reaction of $C_{10}H_{15}O_7 \cdot$ with $HO_2 \cdot$ most likely accounts for the significant increase of $C_{10}H_{16}O_7$. Similarly, species in the $C_{10}H_{16}O_x$ family that have more than seven oxygen atoms can be attributed to reactions of $C_{10}H_{15}O_x \cdot$
290 peroxy radicals with $HO_2 \cdot$.

The $C_{10}H_{17}O_7 \cdot$ peroxy radicals exhibit a rapid formation rate and a high molar yield in α -pinene photooxidation, and the formation is not strongly dependent on NO concentration. This is to be expected when the four-carbon ring is broken on $\cdot OH$ addition (Lee et al., 2023; Piletic and Kleindienst, 2022). Contributions from peroxy radicals containing more than seven oxygen atoms to the $C_{10}H_{17}O_x \cdot$ family are negligible, which is consistent with the number of oxygen atoms in the observed
295 closed-shell products. This phenomenon is in accordance with previous measurement studies and calculations (Berndt, 2021; Lee et al., 2023). In the no-NO case, compounds with more than seven oxygen atoms account for only 0.1% of the $C_{10}H_{18}O_x$ family, whereas for the low-NO and high-NO cases, compounds with more than eight oxygen atoms contribute 5% and 6%, respectively, to the $C_{10}H_{17}NO_x$ family. Although the fate of the $C_{10}H_{17}O_7 \cdot$ family remains unclear, the product distributions indicate that it is unlikely for them to undergo further steps of autoxidation. However, the $C_{10}H_{15}O_x \cdot$ -related HOM are more
300 oxidized than $C_{10}H_{17}O_x \cdot$ -related HOM. For example, species containing more than eight oxygen atoms in $C_{10}H_{15}NO_x$ account for 43.6% and 46.7% in AN_{low} and AN_{high} cases, respectively, of the entire $C_{10}H_{15}NO_x$ family. Obviously $C_{10}H_{15}O_x \cdot$ isomers with $x \geq 7$ are formed, which exhibit faster unimolecular reaction rates than the accessible isomers of the $C_{10}H_{17}O_x \cdot$ peroxy radicals.

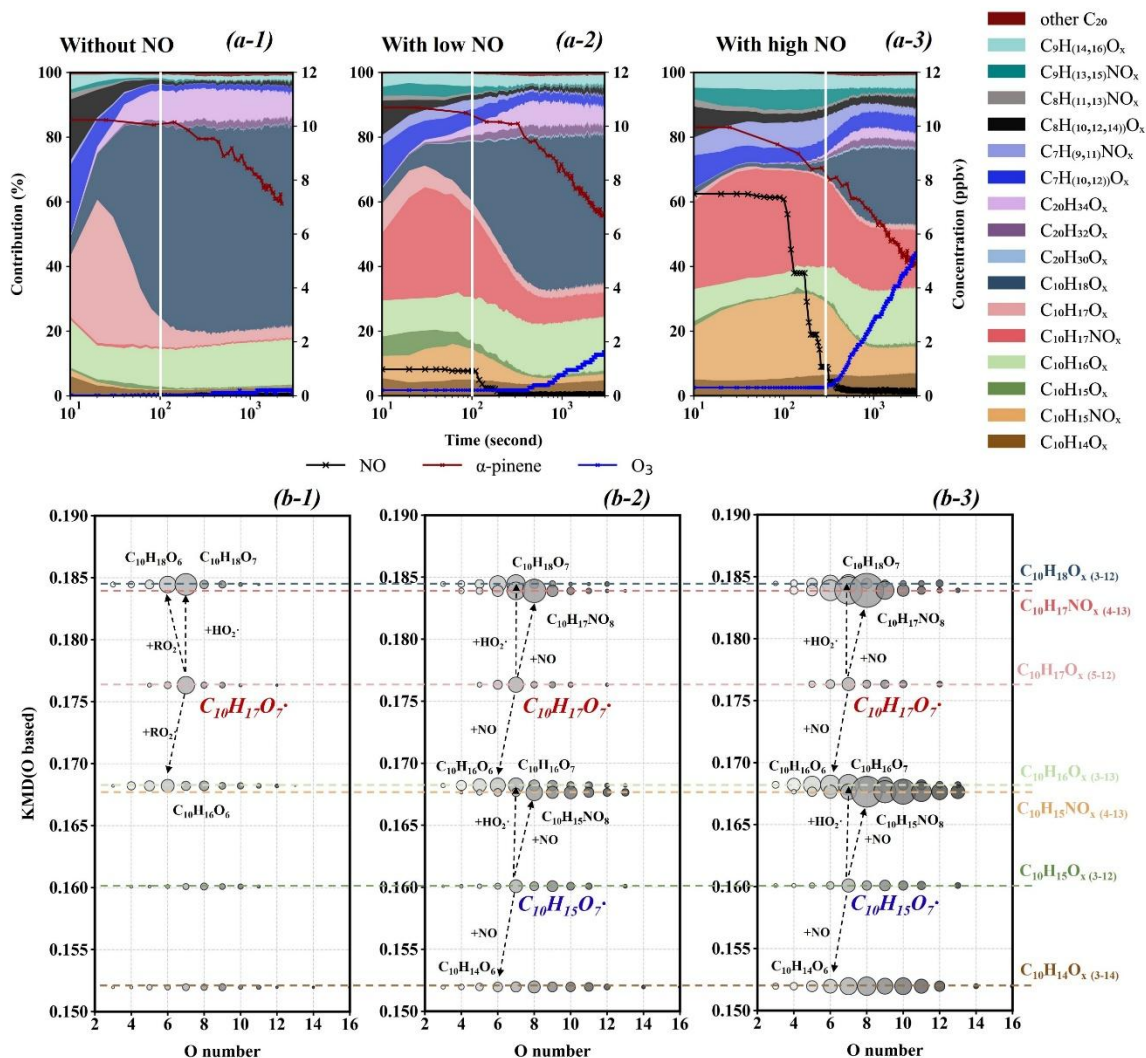
The distribution of the less oxygenated compounds was investigated based on the mass spectra detected by amine-CIMS,
305 which are shown in **Figure S8**. Consistent with nitrate-CIMS, $C_{10}H_{15}O_x \cdot$ -related less oxygenated compounds also emerge with elevated NO concentrations, particularly those in the $C_{10}H_{14}O_x$ and $C_{10}H_{15}NO_x$ families. The dominant compounds in



the $C_{10}H_{15}NO_x$ family are $C_{10}H_{15}NO_4$, $C_{10}H_{15}NO_6$, and $C_{10}H_{15}NO_8$, which should be derived from reaction R6 involving peroxy radicals with the formula $C_{10}H_{15}O_3^{\cdot}$, $C_{10}H_{15}O_5^{\cdot}$, and $C_{10}H_{15}O_7^{\cdot}$, respectively. Among the major compounds in the $C_{10}H_{15}NO_x$ family detected by amine-CIMS only highly oxidized species with the formula $C_{10}H_{15}NO_8$ can also be detected in significant amounts by nitrate-CIMS. The same phenomenon can also be seen for $C_{10}H_{17}O_x^{\cdot}$ -related compounds. In amine-CIMS, the first-generation peroxy radical, $C_{10}H_{17}O_3^{\cdot}$, and its associated closed-shell products play a dominant role in the combined $C_{10}H_{17}O_x^{\cdot}$, $C_{10}H_{18}O_x$, and $C_{10}H_{17}NO_x$ families, although the $C_{10}H_{17}O_7^{\cdot}$ related products are dominant in the mass spectrum obtained by nitrate-CIMS. For example, $C_{10}H_{17}NO_4$ and $C_{10}H_{18}O_3$ are major peaks, which are produced mechanistically through termination reactions of $C_{10}H_{17}O_3^{\cdot}$ by NO and by HO_2^{\cdot} radicals, respectively. $C_{10}H_{17}NO_4$ contribute 56.6% and 57.5% to the $C_{10}H_{17}NO_x$ family in AN_{low} and AN_{high} conditions, respectively. $C_{10}H_{18}O_3$ accounts for 70.6%, 77.6%, and 69.3% in A0, AN_{low} , and AN_{high} cases, respectively.

The fate of $C_{10}H_{17}O_3^{\cdot}$ with the four-membered ring retained is different from $C_{10}H_{17}O_3^{\cdot}$ with four-membered ring opened, since only ring-opened $C_{10}H_{17}O_3^{\cdot}$ can undergo fast autoxidation reactions to produce HOM (Xu et al., 2019). The nitrate-CIMS technique ionizes specifically highly oxygenated organics (Ehn et al., 2014), resulting in the detection of only a narrow range of highly oxidized compounds derived from four ring-opened $C_{10}H_{17}O_3^{\cdot}$. However, four ring-opened $C_{10}H_{17}O_3^{\cdot}$ peroxy radicals account only for approximately 25% of the sum of $C_{10}H_{17}O_3^{\cdot}$ peroxy radicals derived from the OH-addition pathway (Vereecken et al., 2007). The amine-CIMS is efficient in detecting a large range of products including less oxygenated compounds ($O < 7$) (Berndt, 2021). $C_{10}H_{16}O_2(C_3H_7NH_3^+)$ is found to be the strongest peak among the entire mass spectrum in amine-CIMS, indicating the production of pinonaldehyde. Pinonaldehyde can be formed from the formation of alkoxy radicals via reactions of four-membered ring-retained $C_{10}H_{17}O_3^{\cdot}$ peroxy radicals and NO, which then undergo a fast opening of the six membered ring (Rolletter et al., 2019). Therefore, the inclusion of products from both four ring-retained and four ring-opened $C_{10}H_{17}O_3^{\cdot}$ peroxy radicals in amine-CIMS can explain the difference in the product distributions detected by nitrated-CIMS and by amine-CIMS.

In conclusion, the product distributions from α -pinene photooxidation during early reaction stages were investigated. Compared to no-NO conditions, the presence of NO enhanced the formation of organic nitrates and promoted alkoxy formation steps, which lead to significant formation of $C_{10}H_{15}O_x^{\cdot}$ -related compounds. These were detected by both nitrate-CIMS and amine-CIMS. The initial peroxy radicals leading to $C_{10}H_{15}O_x^{\cdot}$ related products were identified as $C_{10}H_{15}O_3^{\cdot}$, which cannot arise from ozonolysis of α -pinene since O_3 formation is negligible in the early reaction stages, as illustrated in **Figure 2**. Also, $C_{10}H_{15}O_4^{\cdot}$ peroxy radicals are mechanistically expected to be first generation peroxy radicals in ozonolysis. Potential mechanisms that could be responsible for the emergence of $C_{10}H_{15}O_x^{\cdot}$ -related HOM will be discussed in the following section.



340 **Figure 2.** Panels (a-1, a-2, a-3) show stacked figures with the contributions of each product family from α -pinene photooxidation as a function of reaction time. The families representing major monomers (C = 10), fragments (C < 10), and accretion products (C = 20) are included in panels (a-1, a-2, a-3). Time series of concentrations for α -pinene, NO, and O₃ are also presented. The corresponding panels (b-1, b-2, b-3) located below each stack plot show the Kendrick Mass Defect (KMD, based on oxygen weight) of monomer compounds as a function of oxygen number, with marker sizes indicating the relative abundance of each compound in the early reaction stages (0-100s, 0-100s, and 0-300s after reaction starts for b-1, b-2, and b-3, respectively). This is also indicated by the vertical white lines in a-1, a-2, and a-3). Compounds aligned along the same horizontal dashed lines are in same family, with the same carbon and hydrogen number but differing in oxygen number. Family names are shown on the right. The texts in panels (b-1, b-2, b-3) highlight major compounds with high abundance and their possible formation pathways. NO conditions increase in the panels from left to right, from no-NO and low-NO to high-NO, respectively. The products here are detected by nitrate-CIMS.

345

350



355

3.2 C₁₀H₁₅O_x-related HOM is attributed to H-abstraction pathway

In α -pinene oxidation systems three possible pathways can lead to monomers with 15 hydrogen atoms: either the H-abstraction channel by $\cdot\text{OH}$ radicals (Shen et al., 2022), ozonolysis (Berndt, 2022), or oxidation of pinonaldehyde (Rolletter et al., 2020). However, as mentioned in section 3.1, ozone was not present at the beginning of each transient cycle and could not accumulate sufficiently during early reaction stages, and thus cannot account for the formation of C₁₀H₁₅O_x-related products. To explore potential formation pathways of C₁₀H₁₅O_x-related compounds in α -pinene photooxidation systems in presence of NO, FCM clustering was applied to the time series of 156 ions detected by nitrate-CIMS and amine-CIMS. Selection criteria for the ions were contributions of more than 0.1% to the total ion signal in nitrate-CIMS or more than 1% to the total ion signal in amine-CIMS.

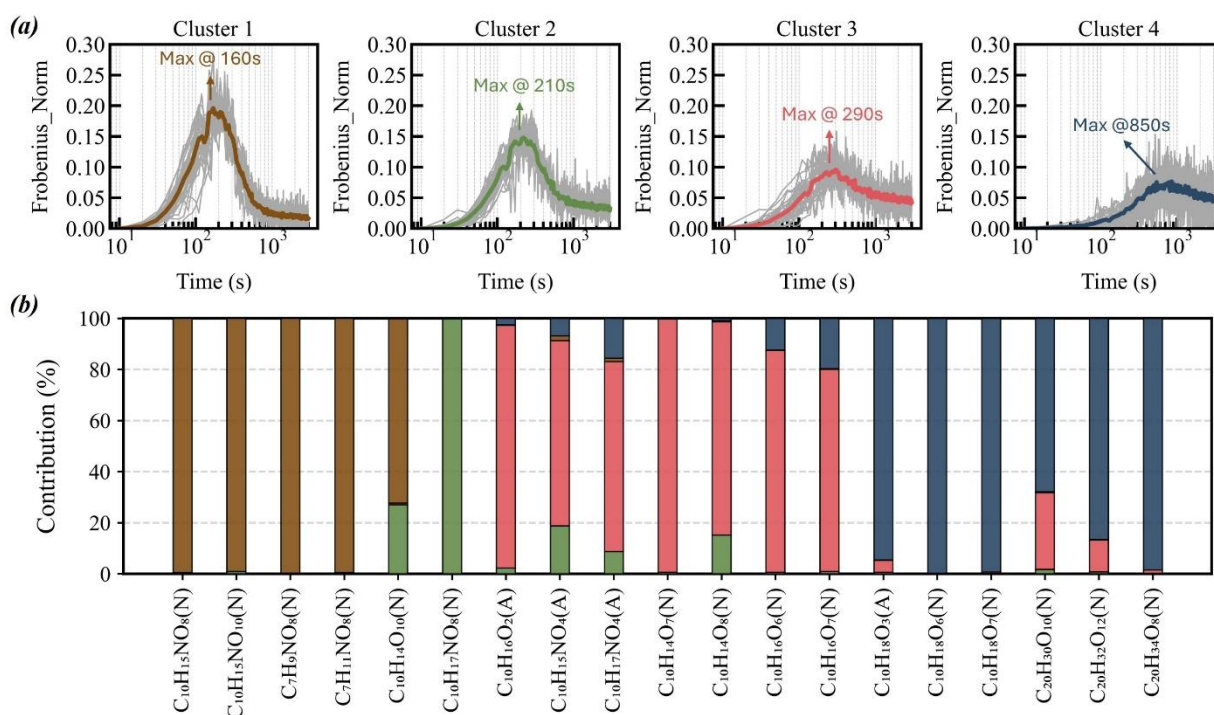
A four-cluster solution was identified as the optimal solution. Corresponding results are presented in **Figure 3**. **Figure 3(a)** shows the time series of the four cluster centers and the contributing ions. Compounds in cluster 1 form immediately after reactions are initiated by switching on the UV-C lamps, followed by cluster 2 and cluster 3, while compounds in cluster 4 need longest time to be formed. The cluster centers peak at approximately 160s, 210s, 290s, and 850s, respectively. As shown in **Figure 3(b)**, the major monomers in the C₁₀H₁₈O_x family and the major dimers (C₂₀H₃₀O_x, C₂₀H₃₂H₁₂, C₂₀H₃₄O₈) are all found in cluster 4, which exhibits the slowest formation rate among four clusters. These compounds originate from biomolecular termination reactions (reaction R1 and R5), with their production rates largely controlled by the concentration of HO₂ \cdot and RO₂ \cdot radicals. NO is already in a steady state in the dark chamber, while HO₂ \cdot and RO₂ \cdot only begin to accumulate after the UV-C lamps are switched on. Therefore, the RO₂ \cdot fate is immediately affected by NO. Consequently, under AN_{high} conditions RO₂ \cdot + NO reactions as well as autoxidation play a dominant role for the RO₂ \cdot in early reactions, and only these two reactions are discussed in following sections.

Compounds in cluster 1 and cluster 2 initially increase dramatically before decreasing again, and cluster 1 exhibits a steeper decline than cluster 2. The bulk chemical properties and the average carbon oxidation state (\overline{OSc}) of each cluster are calculated (Kroll et al., 2011; Wu et al., 2021) and plotted as a function of average carbon (n_C) or nitrogen atoms (n_N) (**Figure S9**). The early-generation cluster 1 exhibits the highest \overline{OSc} and n_N but the lowest n_C , indicating that it mainly consists of highly oxidized nitrogen-containing compounds and fragments ($C < 10$). This characteristic distinguishes cluster 1 from the other clusters. It is determined by the emerging of $\cdot\text{OH}$ radicals at elevated NO concentration in the early stage.

The formation rate of each cluster can be interpreted kinetically as 'typical' chemical formation rate (Wu et al., 2024). The compounds C₁₀H₁₅NO₇(NO₃⁻) and C₁₀H₁₅NO₈(NO₃⁻) are assigned to cluster 1 with the fastest formation rate; thus, they should be first generation products. Pinonaldehyde (C₁₀H₁₆O₂(C₃H₇NH₃⁺)), a possible precursor, can only be found in cluster 3, which has a much slower formation rate. This clearly shows that pinonaldehyde oxidation cannot explain the production



of $C_{10}H_{15}NO_7(NO_3^-)$ or $C_{10}H_{15}NO_8(NO_3^-)$. $C_7H_9NO_8(NO_3^-)$, which is detected in high amount in nitrate-CIMS and also attributed to cluster 1, went through a fragmentation step and is possibly formed via decomposition of $C_{10}H_{15}O_x$, followed by further autoxidation and termination reactions by NO (Shen et al., 2022). Therefore, H-abstraction is probably the reason for the significant formation of $C_{10}H_{15}O_x$ -related HOM, and not the oxidation of pinonaldehyde. The fragment $C_7H_{11}NO_8(NO_3^-)$ is formed faster than the organic nitrate monomer $C_{10}H_{17}NO_8(NO_3^-)$, even though both of them are initialized by the OH-addition channel. This relation differs from that of $C_7H_9NO_8(NO_3^-)$ and $C_{10}H_{15}NO_8(NO_3^-)$. High NO can promote the alkoxy radical formation and its isomerization, which is crucial to form C_7 fragments and ring-opened peroxy radicals in α -pinene photooxidation system (Berndt, 2021; Vereecken and Peeters, 2000). However, to form $C_{10}H_{17}O_7$ peroxy radicals two steps of autoxidation are required. Those can be suppressed at high NO, since NO reacts fast with RO_2 via reaction R6 and R7 (Berndt, 2021; Piletic and Kleindienst, 2022). In other words, the fast NO-related reactions in early stages are most likely the reason for the emergence of compounds in cluster 1, while NO-unrelated reactions cannot compete.



400 **Figure 3.** Results of fuzzy c-means clustering for the dominant peaks (156 in total) during early reaction stages of α -pinene photooxidation under high NO condition are shown in panel (a). The four-cluster solution is shown here. The time series of the cluster centers are displayed as colored solid lines, while individual species are shown in gray lines. Panel (b) illustrates the cluster apportionment of selected major products detected in both nitrated-CIMS (N) and amine-CIMS (A).



405 To assess the potential contribution of pinonaldehyde oxidation to the formation of $C_{10}H_{15}O_x$ -related HOM, pinonaldehyde photooxidation experiments were conducted under no-NO and high NO conditions, analogous to conditions applied in the α -pinene systems (**Table 1**). Time series of NO (ppbv), α -pinene (ppbv), and pinonaldehyde as product (in ncps) under AN_{high} conditions are shown in **Figure 4 (a-1)**. The time series of pinonaldehyde (as precursor; in ncps) and NO (ppbv) under PN_{high} conditions are plotted in **Figure 4 (a-2)**. The major $C_{10}H_{15}O_x$ -related products derived from AN_{high} (dark color) and PN_{high} (bottom) are shown in the bar plots (**Figure 4 (b)**), where major products ($C_{10}H_{14}O_x$ and $C_{10}H_{15}NO_x$ family) detected by both nitrate-CIMS (in red) and amine-CIMS (in blue) are displayed. As shown in **Table 1**, concentrations of $\cdot OH$ radicals are 7.5×10^6 mole cm^{-3} and 9.3×10^6 mole cm^{-3} in AN_{high} and PN_{high} conditions, respectively. The estimated pinonaldehyde turnover under PN_{high} conditions is ~ 11 times the turnover as product under AN_{high} conditions. For $C_{10}H_{15}O_x$ -related HOM detected by nitrate-CIMS, the summed signal of $C_{10}H_{14}O_x$ and $C_{10}H_{15}NO_x$ under AN_{high} conditions are 3.9 times and 2 times higher, respectively, compared to those under PN_{high} conditions. For less oxygenated compounds detected by amine-CIMS, the summed concentrations of $C_{10}H_{14}O_x$ and $C_{10}H_{15}NO_x$ under AN_{high} conditions are 21.4 and 0.56 times those under PN_{high} conditions. None of these ratios are comparable to the ratio of the pinonaldehyde turnover in the two systems, indicating that the absolute intensity of $C_{10}H_{15}O_x$ -related HOM formed under the AN_{high} conditions cannot be solely explained by photooxidation of pinonaldehyde.

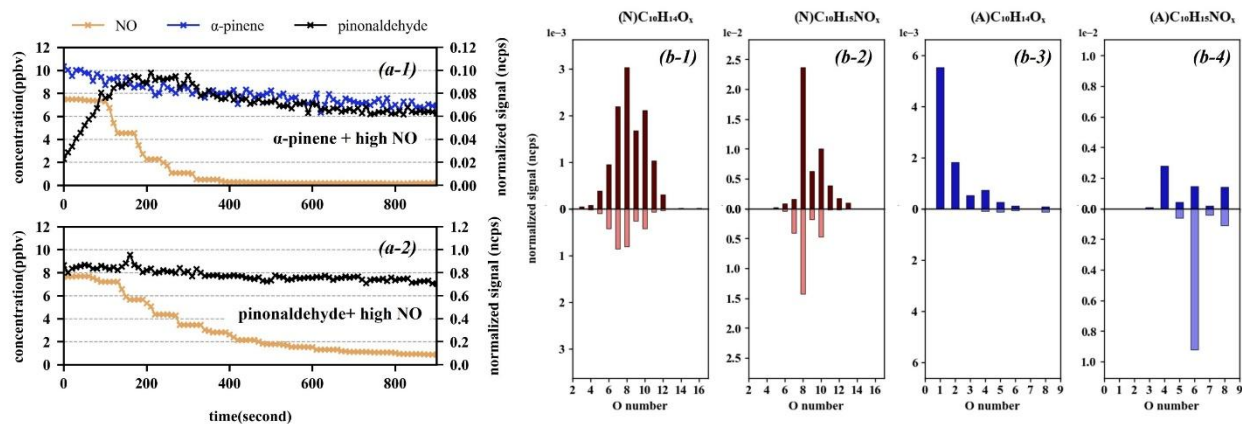
420 For highly oxygenated compounds in nitrate-CIMS, species containing more than 10 oxygen atoms account for 11% of the $C_{10}H_{14}O_x$ family and 13% of the $C_{10}H_{15}NO_x$ family under AN_{high} conditions, whereas their contributions are much lower under PN_{high} conditions (4% and 1.2%, respectively). The initial NO concentrations (**Table 1**) for two conditions are comparable, and consequently autoxidation rates can be the reason responsible for the differences in HOM distributions. Therefore, for peroxy radicals with more than 9 oxygen atoms the autoxidation chain of $C_{10}H_{15}O_x$ peroxy radicals in pinonaldehyde photooxidation experiments is more easily terminated by NO than for peroxy radicals resulting from α -pinene photooxidation systems. The difference in the product distributions is significant between the two systems. In the PN_{high} system, the intensity of the $C_{10}H_{14}O_x$ family is lower than that of the $C_{10}H_{15}NO_x$ family, indicating that the branching towards reaction R8 undergoing self-termination is lower than the branching towards reaction R6.

430 For less oxygenated compounds detected by amine-CIMS, the most abundant species in $C_{10}H_{15}NO_x$ family, $C_{10}H_{15}NO_4$, derived from the reaction of $C_{10}H_{15}O_3$ peroxy radicals with NO under AN_{high} conditions, does not appear in the PN_{high} system. Primary peroxy radicals with a formula of $C_{10}H_{15}O_4$ are formed when $\cdot OH$ abstracts a hydrogen atom, mainly from the aldehyde group in pinonaldehyde (Rolletter et al., 2020; Fantechi et al., 2002), as a prerequisite for autoxidation. $C_{10}H_{15}O_3$ form when $\cdot OH$ radicals abstract a hydrogen atom from α -pinene molecules, followed an alkoxy step (reaction R7), a 6-membered ring opening, and an O_2 molecule addition (Shen et al., 2022). Here, the appearance of $C_{10}H_{15}NO_4$ could be explained by termination reactions between $C_{10}H_{15}O_3$ and NO in the AN_{high} system, when the H-abstraction pathway indeed exists. The species detected in amine-CIMS with the formula $C_{10}H_{15}NO_6$ are significantly higher than other compounds in the $C_{10}H_{15}NO_x$ family under PN_{high} conditions. These species are less important than $C_{10}H_{15}NO_4$ under AN_{high} conditions. If an alkoxy radical is formed by the reaction of $C_{10}H_{15}O_4$ with NO, followed by H-shift and an O_2 addition,



440 $C_{10}H_{15}O_5$ peroxy radicals will be produced and can be terminated by NO to produce $C_{10}H_{15}NO_6$ species. This is a potential pathway which could be responsible for the significant formation of $C_{10}H_{15}NO_6$ under PN_{high} conditions.

In summary, clustering analysis shows that $C_{10}H_{15}NO_x$ HOM species exhibit the fastest formation rate among all HOM compounds. They are also faster than first-generation product generation (e.g., pinonaldehyde) in the OH-addition channel under AN_{high} conditions. The intensity of $C_{10}H_{15}O_x$ related HOM in the α -pinene photooxidation system was much higher than in the pinonaldehyde photooxidation system, despite the estimated pinonaldehyde turnover in α -pinene system being
 445 less than 10% of that in the pinonaldehyde photooxidation system. Additionally, product distributions observed in the α -pinene system differ substantially from those in the pinonaldehyde system, regardless of whether they are detected by nitrate-CIMS or amine-CIMS. Therefore, these findings demonstrate that the H-abstraction pathway, rather than the oxidation of pinonaldehyde, accounts for the formation of $C_{10}H_{15}O_x$ related HOM in the α -pinene system.



450 **Figure 4.** Panel (a-1) displays time series of α -pinene and NO concentrations, along with the normalized signal of pinonaldehyde, representing α -pinene photooxidation under high NO conditions. Panel (a-2) shows time series of NO concentration and the normalized signal of pinonaldehyde measured during pinonaldehyde photooxidation under high NO conditions. Product distributions of $C_{10}H_{15}NO_x$ and $C_{10}H_{14}O_x$ families are shown in panels (b-1) to (b-4), where red and blue bars represent data detected by nitrate-CIMS and amine-CIMS, respectively. Results from α -pinene photooxidation and
 455 pinonaldehyde photooxidation are shown in the top and bottom half of panels (b-1) to (b-4).



4. Conclusions and Atmospheric Implications

In this study a series of photooxidation experiments was conducted under varying NO levels to investigate the effect of NO on the $C_{10}H_{15}O_x$ -related HOM formation in the α -pinene photooxidation system, and to unravel potential formation pathways of these products. The chemical system was brought to a steady state in the dark. Afterwards, reactions were initiated by photolyzing H_2O_2 . We focused on early reaction stages (the first hundreds of seconds), during which $RO_2\cdot + NO$ reactions and $RO_2\cdot$ autoxidation dominates the fate of the $RO_2\cdot$. The $C_{10}H_{15}O_x$ -related HOM exhibits a strong dependence on NO levels and can only be formed in significant amounts in the presence of NO. In contrast, $C_{10}H_{17}O_x$ -related HOM are dominantly formed via the OH-addition pathway. Product distributions, potential formation pathways, and rates of $C_{10}H_{17}O_x$ -related HOM have been widely and extensively studied (Berndt, 2021; Xu et al., 2019), and our findings on $C_{10}H_{17}O_x$ -related HOM formation are consistent with previous studies. However, potential formation pathways, distributions, and NO dependence of $C_{10}H_{15}O_x$ -related compounds were missing systematic exploration so far. Here we have shown that $C_{10}H_{15}O_x$ -related HOM form mostly via the H-abstraction pathway.

Since the photolysis of H_2O_2 was utilized to produce $\cdot OH$ radicals O_3 did not accumulate during the early reaction stages; therefore, ozonolysis did not interfere with the $\cdot OH$ pathways. FCM analysis proves that the dominant species in the $C_{10}H_{15}NO_x$ family, $C_{10}H_{15}NO_8$ and $C_7H_9NO_8$, can be distinguished from other species by their fast formation rates in the presence of NO. Pinonaldehyde can be excluded as a potential precursor since the related ion was only found in a cluster with slower formation rates. The product distribution of $C_{10}H_{15}O_x$ -related compounds obtained from pinonaldehyde photooxidation differs significantly from that obtained from α -pinene photooxidation, even though all the experiments were conducted under similar $\cdot OH$ and NO conditions. In summary, the findings rule out pinonaldehyde oxidation as a significant source of $C_{10}H_{15}O_x$ -related compounds when NO is present. Therefore, H-abstraction from α -pinene by $\cdot OH$ is the most likely formation pathway.

As illustrated in *Figure S10* and *Figure S11*, the contribution of the H-abstraction pathway to HOM formation increases with elevated NO levels compared to the OH-addition pathway. The ratios between major $C_{10}H_{15}O_x$ -related HOM and $C_{10}H_{17}O_x$ -related HOM rise with increasing NO concentrations. The ratios of $C_{10}H_{15}O_x$ peroxy radicals to $C_{10}H_{17}O_x$ peroxy radicals are 0.09, 0.71, and 1.4 under no-NO, low-NO, and high-NO conditions, respectively. Similarly, the ratio of $C_{10}H_{15}NO_x$ to $C_{10}H_{17}NO_x$ increases from 0.34 to 0.84 when NO levels increase from low to high. The sum of the major $C_{10}H_{15}O_x$ -related closed-shell HOM ($C_{10}H_{14}O_x$ and $C_{10}H_{15}NO_x$) contributes around 30% to total HOM under high NO conditions. The contribution of the H-abstraction related products observed in this study is 70 % lower than that reported by Shen et al. (Shen et al., 2022). The discrepancy may arise from differences in measurement techniques: Shen et al. (Shen et al., 2022) used an Eisele type inlet (Mauldin et al., 1999), while in this study a MION inlet was used (Rissanen et al., 2019). Notably, we observed that less oxygenated HOM (less than eight oxygen atoms) dominate the $C_{10}H_{17}O_x$ -related HOM family. In contrast, higher oxygenated HOM (more than eight oxygen atoms) play a greater role in the study of Shen et al. (Shen et al., 2022). Consequently, underestimating the contribution of less oxygenated $C_{10}H_{17}O_x$ -related HOM would result



in overestimating the contribution of $C_{10}H_{15}O_x$ -related HOM. Therefore, a comparison between the two inlet types may be
490 of interest to the HOM community in the future.

These findings indicate that the HOM yield attributed to the H-abstraction pathway compared to the OH-addition pathway
can be significant, and should not be overlooked when assessing the importance of HOM in SOA formation, especially in the
presence of NO. Comprehensive product distributions formed through the H-abstraction pathway in α -pinene oxidation are
illustrated in this study. HOM species with the formula $C_{10}H_{15}NO_8$, recognized as characteristic indicators of OH \cdot initiated
495 monoterpene oxidation in presence of NO under daytime atmospheric conditions (Yan et al., 2016; Kulmala et al., 2013),
can potentially be attributed to the H-abstraction pathway. Therefore, the contribution of the H-abstraction channel to HOM
formation should be highlighted, especially under high NO conditions, which frequently can be observed in megacities. The
presence of NO not only terminates peroxy radicals and suppresses HOM formation, but also propagates the oxidative
radical chain through the formation of alkoxy radicals and their subsequent isomerization, a process that under high NO
500 levels can even compete with autoxidation (Kang et al., 2025). These reactions lead to effective NO-NO₂ conversion and can
then become a crucial step to promote O₃ formation. The occurrence of alkoxy steps can also directly be related to O₃
formation in addition to O₃ sensitivity via the ratio of organic nitrate and non-nitrate HOM (Zhang et al., 2024). However,
branching ratios towards alkoxy radical formation remain uncertain, when RO₂ \cdot reacts with NO. Further investigation is
needed to clarify the role of alkoxy processes in both SOA and O₃ formation.



505 **Author contributions**

HW and HS prepared the manuscript with contributions by SK, TFM, DRW, DZ, and SRZ. HW, AZ, MB, YB, RW, SK, QH, TH, and SRZ conducted the experiments and performed the measurements. HW, HS, and SK analyzed the data. HW performed the model calculations. The compiled data set was interpreted by HW, HS, DZ, and SRZ. All co-authors discussed the results and commented on the manuscript.

510 **Data availability**

The data is available upon request. For the published version the data will be available from a repository.

Competing interests

The authors declare no competing financial interest. One of the authors is a member of the editorial board of ACP.

Financial support

515 This research was supported by the Federal Ministry of Education and Research (BMBF, Germany) under the FONA strategy “Research for Sustainability” through the ACTRIS-D project (funding code: 01LK200010). Hongru Shen and Defeng Zhao would like to thank for funding support from the Shanghai Pilot Program for Basic Research-Fudan University 21TQ1400100 (22TQ010).

References

- 520 Albrecht, S. R., Novelli, A., Hofzumahaus, A., Kang, S., Baker, Y., Mentel, T., Wahner, A., and Fuchs, H.: Measurements of hydroperoxy radicals (HO₂) at atmospheric concentrations using bromide chemical ionisation mass spectrometry, *Atmospheric Measurement Techniques*, 12, 891-902, 10.5194/amt-12-891-2019, 2019.
- Atkinson, R. and Arey, J.: Atmospheric Degradation of Volatile Organic Compounds, *Chemical Reviews*, 103, 4605-4638, 10.1021/cr0206420, 2003.
- 525 Baker, Y., Kang, S., Wang, H., Wu, R., Xu, J., Zanders, A., He, Q., Hohaus, T., Ziehm, T., Geretti, V., Bannan, T. J., O'Meara, S. P., Voliotis, A., Hallquist, M., McFiggans, G., Zorn, S. R., Wahner, A., and Mentel, T. F.: Impact of HO₂ / RO₂ ratio on highly oxygenated α -pinene photooxidation products and secondary organic aerosol formation potential, *Atmos. Chem. Phys.*, 24, 4789-4807, 10.5194/acp-24-4789-2024, 2024.
- 530 Berndt, T.: Peroxy Radical Processes and Product Formation in the OH Radical-Initiated Oxidation of alpha-Pinene for Near-Atmospheric Conditions, *J Phys Chem A*, 125, 9151-9160, 10.1021/acs.jpca.1c05576, 2021.
- 535 Berndt, T.: Peroxy Radical and Product Formation in the Gas-Phase Ozonolysis of alpha-Pinene under Near-Atmospheric Conditions: Occurrence of an Additional Series of Peroxy Radicals O₂C(10)H(15)O(O(2))(y)O(2) with y = 1-3, *J Phys Chem A*, 126, 6526-6537, 10.1021/acs.jpca.2c05094, 2022.



- 540 Berndt, T., Mentler, B., Scholz, W., Fischer, L., Herrmann, H., Kulmala, M., and Hansel, A.: Accretion Product Formation from Ozonolysis and OH Radical Reaction of alpha-Pinene: Mechanistic Insight and the Influence of Isoprene and Ethylene, *Environ Sci Technol*, 52, 11069-11077, 10.1021/acs.est.8b02210, 2018.
- 545 Berndt, T., Richters, S., Jokinen, T., Hyttinen, N., Kurten, T., Otkjaer, R. V., Kjaergaard, H. G., Stratmann, F., Herrmann, H., Sipila, M., Kulmala, M., and Ehn, M.: Hydroxyl radical-induced formation of highly oxidized organic compounds, *NATURE COMMUNICATIONS*, 7, 10.1038/ncomms13677, 2016.
- 550 Bianchi, F., Kurten, T., Riva, M., Mohr, C., Rissanen, M. P., Roldin, P., Berndt, T., Crouse, J. D., Wennberg, P. O., Mentel, T. F., Wildt, J., Junninen, H., Jokinen, T., Kulmala, M., Worsnop, D. R., Thornton, J. A., Donahue, N., Kjaergaard, H. G., and Ehn, M.: Highly Oxygenated Organic Molecules (HOM) from Gas-Phase Autoxidation Involving Peroxy Radicals: A Key Contributor to Atmospheric Aerosol, *CHEMICAL REVIEWS*, 119, 3472-3509, 10.1021/acs.chemrev.8b00395, 2019.
- 555 Campello, R. J. G. B. and Hruschka, E. R.: A fuzzy extension of the silhouette width criterion for cluster analysis, *Fuzzy Sets and Systems*, 157, 2858-2875, 10.1016/j.fss.2006.07.006, 2006.
- 560 Ehn, M., Thornton, J. A., Kleist, E., Sipila, M., Junninen, H., Pullinen, I., Springer, M., Rubach, F., Tillmann, R., Lee, B., Lopez-Hilfiker, F., Andres, S., Acir, I. H., Rissanen, M., Jokinen, T., Schobesberger, S., Kangasluoma, J., Kontkanen, J., Nieminen, T., Kurten, T., Nielsen, L. B., Jorgensen, S., Kjaergaard, H. G., Canagaratna, M., Maso, M. D., Berndt, T., Petaja, T., Wahner, A., Kerminen, V. M., Kulmala, M., Worsnop, D. R., Wildt, J., and Mentel, T. F.: A large source of low-volatility secondary organic aerosol, *Nature*, 506, 476-479, 10.1038/nature13032, 2014.
- 565 Fantechi, G., Vereecken, L., and Peeters, J.: The OH-initiated atmospheric oxidation of pinonaldehyde: Detailed theoretical study and mechanism construction Electronic supplementary information (ESI) available: quantum chemical and RRKM results. See <http://www.rsc.org/suppdata/cp/b2/b205901k>, *Physical Chemistry Chemical Physics*, 4, 5795-5805, 10.1039/b205901k, 2002.
- 570 Iyer, S., Reiman, H., Moller, K. H., Rissanen, M. P., Kjaergaard, H. G., and Kurten, T.: Computational Investigation of RO(2) + HO(2) and RO(2) + RO(2) Reactions of Monoterpene Derived First-Generation Peroxy Radicals Leading to Radical Recycling, *J Phys Chem A*, 122, 9542-9552, 10.1021/acs.jpca.8b09241, 2018.
- 575 Jenkin, M. E., Saunders, S. M., and Pilling, M. J.: The tropospheric degradation of volatile organic compounds: a protocol for mechanism development, *Atmospheric Environment*, 31, 81-104, [https://doi.org/10.1016/S1352-2310\(96\)00105-7](https://doi.org/10.1016/S1352-2310(96)00105-7), 1997.
- 580 Jenkin, M. E., Valorso, R., Aumont, B., and Rickard, A. R.: Estimation of rate coefficients and branching ratios for reactions of organic peroxy radicals for use in automated mechanism construction, *Atmospheric Chemistry and Physics*, 19, 7691-7717, 10.5194/acp-19-7691-2019, 2019.
- 585 Jimenez, J. L., Canagaratna, M. R., Donahue, N. M., Prevot, A. S. H., Zhang, Q., Kroll, J. H., DeCarlo, P. F., Allan, J. D., Coe, H., Ng, N. L., Aiken, A. C., Docherty, K. S., Ulbrich, I. M., Grieshop, A. P., Robinson, A. L., Duplissy, J., Smith, J. D., Wilson, K. R., Lanz, V. A., Hueglin, C., Sun, Y. L., Tian, J., Laaksonen, A., Raatikainen, T., Rautiainen, J., Vaattovaara, P., Ehn, M., Kulmala, M., Tomlinson, J. M., Collins, D. R., Cubison, M. J., Dunlea, E. J., Huffman, J. A., Onasch, T. B., Alfarra, M. R., Williams, P. I., Bower, K., Kondo, Y., Schneider, J., Drewnick, F., Borrmann, S., Weimer, S., Demerjian, K., Salcedo, D., Cottrell, L., Griffin, R., Takami, A., Miyoshi, T., Hatakeyama, S., Shimono, A., Sun, J. Y., Zhang, Y. M., Dzepina, K., Kimmel, J. R., Sueper, D., Jayne, J. T., Herndon, S. C., Trimborn, A. M., Williams, L. R., Wood, E. C., Middlebrook, A. M., Kolb, C. E., Baltensperger, U., and Worsnop, D. R.: Evolution of Organic Aerosols in the Atmosphere, *SCIENCE*, 326, 1525-1529, 10.1126/science.1180353, 2009.



- Kang, S., Wildt, J., Pullinen, I., Vereecken, L., Wu, C., Wahner, A., Zorn, S. R., and Mentel, T. F.: Formation of highly oxygenated organic molecules from α -pinene photooxidation: evidence for the importance of highly oxygenated alkoxy radicals, *EGUsphere*, 2025, 1-33, [10.5194/egusphere-2025-2772](https://doi.org/10.5194/egusphere-2025-2772), 2025.
- 590 Kiendler-Scharr, A., Wildt, J., Dal Maso, M., Hohaus, T., Kleist, E., Mentel, T. F., Tillmann, R., Uerlings, R., Schurr, U., and Wahner, A.: New particle formation in forests inhibited by isoprene emissions, *Nature*, 461, 381-384, [10.1038/nature08292](https://doi.org/10.1038/nature08292), 2009.
- 595 Koss, A. R., Canagaratna, M. R., Zaytsev, A., Krechmer, J. E., Breitenlechner, M., Nihill, K. J., Lim, C. Y., Rowe, J. C., Roscioli, J. R., Keutsch, F. N., and Kroll, J. H.: Dimensionality-reduction techniques for complex mass spectrometric datasets: application to laboratory atmospheric organic oxidation experiments, *Atmos Chem Phys*, 20, 1021-1041, [10.5194/acp-20-1021-2020](https://doi.org/10.5194/acp-20-1021-2020), 2020.
- 600 Kroll, J. H., Donahue, N. M., Jimenez, J. L., Kessler, S. H., Canagaratna, M. R., Wilson, K. R., Altieri, K. E., Mazzoleni, L. R., Wozniak, A. S., Bluhm, H., Mysak, E. R., Smith, J. D., Kolb, C. E., and Worsnop, D. R.: Carbon oxidation state as a metric for describing the chemistry of atmospheric organic aerosol, *NATURE CHEMISTRY*, 3, 133-139, [10.1038/NCHEM.948](https://doi.org/10.1038/NCHEM.948), 2011.
- 605 Kulmala, M., Kontkanen, J., Junninen, H., Lehtipalo, K., Manninen, H. E., Nieminen, T., Petäjä, T., Sipilä, M., Schobesberger, S., Rantala, P., Franchin, A., Jokinen, T., Järvinen, E., Äijälä, M., Kangasluoma, J., Hakala, J., Aalto, P. P., Paasonen, P., Mikkilä, J., Vanhanen, J., Aalto, J., Hakola, H., Makkonen, U., Ruuskanen, T., Mauldin, R. L., Duplissy, J., Vehkamäki, H., Bäck, J., Kortelainen, A., Riipinen, I., Kurtén, T., Johnston, M. V., Smith, J. N., Ehn, M., Mentel, T. F., Lehtinen, K. E. J., Laaksonen, A., Kerminen, V.-M., and Worsnop, D. R.: Direct Observations of Atmospheric Aerosol Nucleation, *Science*, 339, 943-946, [10.1126/science.1227385](https://doi.org/10.1126/science.1227385), 2013.
- 610 Lee, B. H., Iyer, S., Kurtén, T., Varelas, J. G., Luo, J., Thomson, R. J., and Thornton, J. A.: Ring-opening yields and auto-oxidation rates of the resulting peroxy radicals from OH-oxidation of α -pinene and β -pinene, *Environmental Science: Atmospheres*, 3, 399-407, [10.1039/d2ea00133k](https://doi.org/10.1039/d2ea00133k), 2023.
- 615 Mauldin, R. L., Tanner, D. J., Heath, J. A., Huebert, B. J., and Eisele, F. L.: Observations of H₂SO₄ and MSA during PEM-Tropics-A, *Journal of Geophysical Research: Atmospheres*, 104, 5801-5816, [10.1029/98jd02612](https://doi.org/10.1029/98jd02612), 1999.
- 620 Mentel, T. F., Springer, M., Ehn, M., Kleist, E., Pullinen, I., Kurtén, T., Rissanen, M., Wahner, A., and Wildt, J.: Formation of highly oxidized multifunctional compounds: autoxidation of peroxy radicals formed in the ozonolysis of alkenes – deduced from structure–product relationships, *Atmospheric Chemistry and Physics*, 15, 6745-6765, [10.5194/acp-15-6745-2015](https://doi.org/10.5194/acp-15-6745-2015), 2015.
- 625 Mentel, T. F., Wildt, J., Kiendler-Scharr, A., Kleist, E., Tillmann, R., Dal Maso, M., Fisseha, R., Hohaus, T., Spahn, H., Uerlings, R., Wegener, R., Griffiths, P. T., Dinar, E., Rudich, Y., and Wahner, A.: Photochemical production of aerosols from real plant emissions, *Atmos. Chem. Phys.*, 9, 4387-4406, [10.5194/acp-9-4387-2009](https://doi.org/10.5194/acp-9-4387-2009), 2009.
- 630 Peng, J., Hu, M., Guo, S., Du, Z., Zheng, J., Shang, D., Levy Zamora, M., Zeng, L., Shao, M., Wu, Y.-S., Zheng, J., Wang, Y., Glen, C. R., Collins, D. R., Molina, M. J., and Zhang, R.: Markedly enhanced absorption and direct radiative forcing of black carbon under polluted urban environments, *Proceedings of the National Academy of Sciences*, 113, 4266-4271, [10.1073/pnas.1602310113](https://doi.org/10.1073/pnas.1602310113), 2016.
- Piletic, I. R. and Kleindienst, T. E.: Rates and Yields of Unimolecular Reactions Producing Highly Oxidized Peroxy Radicals in the OH-Induced Autoxidation of α -Pinene, β -Pinene, and Limonene, *J Phys Chem A*, 126, 88-100, [10.1021/acs.jpca.1c07961](https://doi.org/10.1021/acs.jpca.1c07961), 2022.



- 635 Rissanen, M. P., Mikkilä, J., Iyer, S., and Hakala, J.: Multi-scheme chemical ionization inlet (MION) for fast switching of reagent ion chemistry in atmospheric pressure chemical ionization mass spectrometry (CIMS) applications, *Atmos Meas Tech*, 12, 6635-6646, 10.5194/amt-12-6635-2019, 2019.
- 640 Rissanen, M. P., Kurten, T., Sipila, M., Thornton, J. A., Kangasluoma, J., Sarnela, N., Junninen, H., Jorgensen, S., Schallhart, S., Kajos, M. K., Taipale, R., Springer, M., Mentel, T. F., Ruuskanen, T., Petaja, T., Worsnop, D. R., Kjaergaard, H. G., and Ehn, M.: The formation of highly oxidized multifunctional products in the ozonolysis of cyclohexene, *J Am Chem Soc*, 136, 15596-15606, 10.1021/ja507146s, 2014.
- 645 Rolletter, M., Blocquet, M., Kaminski, M., Bohn, B., Dorn, H.-P., Hofzumahaus, A., Holland, F., Li, X., Rohrer, F., Tillmann, R., Wegener, R., Kiendler-Scharr, A., Wahner, A., and Fuchs, H.: Photooxidation of pinonaldehyde at ambient conditions investigated in the atmospheric simulation chamber SAPHIR, *Atmospheric Chemistry and Physics*, 20, 13701-13719, 10.5194/acp-20-13701-2020, 2020.
- 650 Rolletter, M., Kaminski, M., Acir, I.-H., Bohn, B., Dorn, H.-P., Li, X., Lutz, A., Nehr, S., Rohrer, F., Tillmann, R., Wegener, R., Hofzumahaus, A., Kiendler-Scharr, A., Wahner, A., and Fuchs, H.: Investigation of the α -pinene photooxidation by OH in the atmospheric simulation chamber SAPHIR, *Atmospheric Chemistry and Physics*, 19, 11635-11649, 10.5194/acp-19-11635-2019, 2019.
- 655 Shen, H., Vereecken, L., Kang, S., Pullinen, I., Fuchs, H., Zhao, D., and Mentel, T. F.: Unexpected significance of a minor reaction pathway in daytime formation of biogenic highly oxygenated organic compounds, *Science Advances*, 8, eabp8702, doi:10.1126/sciadv.abp8702, 2022.
- 660 Vereecken, L. and Peeters, J.: Theoretical Study of the Formation of Acetone in the OH-Initiated Atmospheric Oxidation of α -Pinene, *The Journal of Physical Chemistry A*, 104, 11140-11146, 10.1021/jp0025173, 2000.
- Vereecken, L., Muller, J. F., and Peeters, J.: Low-volatility poly-oxygenates in the OH-initiated atmospheric oxidation of alpha-pinene: impact of non-traditional peroxy radical chemistry, *Phys Chem Chem Phys*, 9, 5241-5248, 10.1039/b708023a, 2007.
- 665 Wang, H., Baker, Y., Shen, H. R., Wu, R. R., Kang, S. A., Zhao, D. F., Wahner, A., Zorn, S. R., and Mentel, T. F.: Decomposition of Clusters of Oxygenated Compounds with NO by Applying Voltage Scanning to Chemical Ionization Mass Spectrometry in Steady-State Experiments, *Environmental Science & Technology Letters*, 10.1021/acs.estlett.4c00276, 2024.
- 670 Wu, R., Zorn, S. R., Kang, S., Kiendler-Scharr, A., Wahner, A., and Mentel, T. F.: Application of fuzzy c-means clustering for analysis of chemical ionization mass spectra: insights into the gas phase chemistry of NO₃-initiated oxidation of isoprene, *Atmospheric Measurement Techniques*, 17, 1811-1835, 10.5194/amt-17-1811-2024, 2024.
- 675 Wu, R., Vereecken, L., Tsiligiannis, E., Kang, S., Albrecht, S. R., Hantschke, L., Zhao, D., Novelli, A., Fuchs, H., Tillmann, R., Hohaus, T., Carlsson, P. T. M., Shenolikar, J., Bernard, F., Crowley, J. N., Fry, J. L., Brownwood, B., Thornton, J. A., Brown, S. S., Kiendler-Scharr, A., Wahner, A., Hallquist, M., and Mentel, T. F.: Molecular composition and volatility of multi-generation products formed from isoprene oxidation by nitrate radical, *Atmos Chem Phys*, 21, 10799-10824, 10.5194/acp-21-10799-2021, 2021.
- 680 Xu, L., Moller, K. H., Crouse, J. D., Otkjaer, R. V., Kjaergaard, H. G., and Wennberg, P. O.: Unimolecular Reactions of Peroxy Radicals Formed in the Oxidation of alpha-Pinene and beta-Pinene by Hydroxyl Radicals, *J Phys Chem A*, 123, 1661-1674, 10.1021/acs.jpca.8b11726, 2019.



- 685 Yan, C., Nie, W., Äijälä, M., Rissanen, M. P., Canagaratna, M. R., Massoli, P., Junninen, H., Jokinen, T., Sarnela, N., Häme, S. A. K., Schobesberger, S., Canonaco, F., Yao, L., Prévôt, A. S. H., Petäjä, T., Kulmala, M., Sipilä, M., Worsnop, D. R., and Ehn, M.: Source characterization of highly oxidized multifunctional compounds in a boreal forest environment using positive matrix factorization, *Atmospheric Chemistry and Physics*, 16, 12715-12731, 10.5194/acp-16-12715-2016, 2016.
- 690 Zhang, J., Zhao, J., Luo, Y., Mickwitz, V., Worsnop, D., and Ehn, M.: On the potential use of highly oxygenated organic molecules (HOMs) as indicators for ozone formation sensitivity, *Atmospheric Chemistry and Physics*, 24, 2885-2911, 10.5194/acp-24-2885-2024, 2024.